A switchable circular polarizer based on zenithal bistable liquid crystal gratings

Dimitrios C Zografopoulos[1], Goran Isić[2], Emmanouil E Kriezis[3], and Romeo Beccherelli[1]

[1] Consiglio Nazionale delle Ricerche, Istituto per la Microelettronica e Microsistemi, Via del fosso del cavaliere 100, 00133, Roma, Italy
[2] Center for Solid State Physics and New Materials, Institute of Physics, University of Belgrade, Pregrevica 118, 11080 Belgrade, Serbia
[3] DepartmentDepartment of Electrical and Computer Engineering, Aristotle University of Thessaloniki, Thessaloniki GR-54124, Greece

E-mail: dimitrios.zografopoulos@artov.imm.cnr.it

Abstract. A switchable circular polarizer for infrared telecom wavelengths based on zenithal bistable liquid crystal gratings is designed and investigated by employing the finite-element method for the study of full-wave light propagation and a tensorial formulation for the liquid crystal orientation. The handedness of the output circular polarization can be selected by switching between the two stable states of the liquid-crystal grating. Analysis of the spectral dependence and the tolerance of the polarizer's performance with respect to deviations from the optimized geometry reveals the robustness of its polarizing properties, which stems from the non-resonant nature of its operation.

Keywords: Circular polarizers, nematic liquid crystals, zenithal bistable devices, switchable photonic components. Submitted to: *J. Phys. D*

1. Introduction

Nematic liquid crystals (LC) have been widely exploited in photonics technology as a switchable medium for the design of tunable devices, owing to their large inherent optical anisotropy and the capability of dynamically controlling their optical properties via the application of an external electric signal [1, 2]. Numerous LC-based devices have been thus far demonstrated as key components in applications ranging from the maturely developed display industry to their use as tunable waveguides, filters, and polarizers in planar [3–5] or fiber [6–8] photonics technology platforms.

In typical LC-tunable components, the liquid crystal molecules obtain a certain configuration in the absence of the control signal, which is determined by the geometry, the anchoring conditions, and the physical properties of the materials involved. By applying an external voltage, the LC molecules reorientate, thus changing the spatial profile of the optical anisotropy axis. According to the target application, the control over the LC molecular orientation can tune their polarization-dependent refractive index and, subsequently, the end optical properties of the component, such as resonant wavelengths in filters, polarization rotation, modal birefringence and so forth. In order to achieve tunability, power has to be consumed for the application of the control signal that moves the LC away from its rest condition and maintains the biased LC configuration. Nevertheless, it has been demonstrated that in certain geometries combined with particular boundary conditions, nematic LC can exhibit bistable behaviour, namely the existance of two equilibrium stable states, which correspond to significantly different molecular orientation profiles [9–13]. Such devices attract increased interest in terms of potential applications, since by virtue of their bistable nature control pulses are required only when switching between the two states, thus allowing for zero idle power consumption.

One of the most promising LC bistable structures is the zenithal bistable device (ZBD), which has been commercially exploited in the development of low-cost passively addressed displays for image storing [14]. The ZBD is based on LC cells formed between two surfaces with homeotropic LC anchoring conditions, one of which is patterned with a grating structure of sinusoidal [15–17] or triangular [18] profile. Recently, we have demonstrated that the utility provided by ZBD gratings can be expanded beyond display applications, for instance in the design of switchable beam splitters [19] and steerers [21].

In this work, we describe the design methodology and we investigate the properties of ZBD gratings that operate as switchable quarter waveplates, i.e. the core element in circular polarizers (CP). By alternating between the two stable LC states, the handedness of the output circularly polarized lightwave can be selected. The spectral response of the proposed ZBD-CP is investigated, as well as the tolerance on variations of the geometrical parameters away from the optimal values, revealing robustness due to the non-resonant operation of the device. The selection of the handedness of the output circularly polarized light does not require mechanical rotation of the component, as in static CP based on solid birefrigent materials, nor the application of a control voltage when operating in idle state, as in traditional LC-based waveplates that provide continuous tuning [22]. Thus, these ZBD-CP are envisaged as low-cost, very low power consumption, electrically switchable polarization control elements in, for instance, polarimetric applications, optical microscopy [23], homogeneous circular polarizers [24], glasses and stereoscopic polarizing modulators in 3D projection systems [25, 26], and the control of angular momentum in quantum optical systems [27] or in all-optical magnetic recording [28].

2. Liquid-crystal orientation studies in zenithal bistable gratings

The proposed switchable circular polarizer is based on the structure schematically depicted in Fig. 1. Two identical triangular gratings with lattice pitch p_0 are patterned on dielectric substrates. The base and height of the triangular elements are, respectively, w_0 and a_0. The two gratings are aligned and form a cell, whose thickness h_0 is defined by using dielectric spacers at the border edges of the device, away from its active area. The cell is filled with the nematic mixture E7, typically using capillary forces while the LC is in the isotropic state. The LC is characterized by a birefringence $\Delta n = n_e - n_o$, where n_e and n_o are the extraordinary and ordinary LC indices, respectively. Before the LC infiltration, the surface of the grating

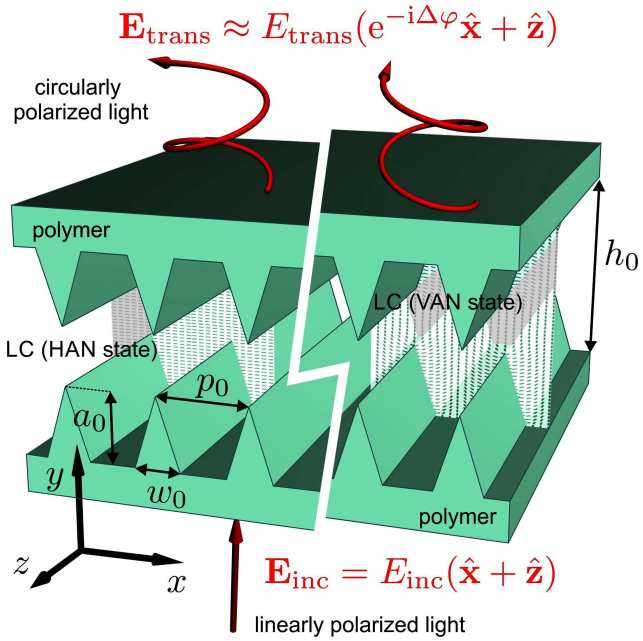

Figure 1. Schematic layout and geometrical parameters of the zenithal bistable liquid-crystal double grating employed for the design of switchable circular polarizers. Triangular grooves are periodically patterned on two identical substrates, which form a liquid-crystal cell that is infiltrated with the nematic mixture E7.

and substrate is treated with a thin layer of surfactant, such as trichloro-alkyl silane [17] or a monomolecular layer of a chrome complex agent [29], which induces homeotropic alignment, i.e. it forces the LC molecules to stay bound perpendicularly to the surface.

The double grating structure employed in this study is an extension of the ZBD gratings, which have been thus far extensively explored thanks to their property of exhibiting two stable LC configurations. The two LC states are associated with a high- and low-tilt average LC orientation, termed as vertical-aligned nematic (VAN) and hybrid-aligned nematic (HAN) states, respectively. In order to investigate the bistability of the proposed gratings, we employ the Q-tensor method, a powerful tool capable of resolving the defect singularities and nematic order parameter variations based on the Landau-de Gennes theory [19, 20].

In this study we follow the formalism and notations explained in detail in [19]. The LC energy and molecular orientation are expressed via the elements q_i and their spatial derivatives ∇q_i of the matrix

$$\mathbf{Q} = \begin{pmatrix} q_1 & q_2 & q_3 \\ q_2 & q_4 & q_5 \\ q_3 & q_5 & -q_1 - q_4 \end{pmatrix}, \tag{1}$$

The $\mathbf{Q}$ matrix is expressed as

$$\mathbf{Q} = S_1 (\mathbf{n} \otimes \mathbf{n}) + S_2 (\mathbf{m} \otimes \mathbf{m}) - \frac{1}{3}(S_1 + S_2)\mathbf{I}, \tag{2}$$

where $\mathbf{I}$ is the unitary matrix and $\mathbf{n}$, $\mathbf{m}$, and $\mathbf{n} \times \mathbf{m}$ are its eigenvectors with corresponding eigenvalues $(2S_1 - S_2)/3$, $(2S_2 - S_1)/3$, and $-(S_1 + S_2)/3$ for the general case of biaxial configurations. Uniaxial solutions exist when two eigenvalues are equal leading to $\mathbf{Q} = S\left[(\mathbf{n} \otimes \mathbf{n}) - (1/3)\mathbf{I}\right]$.

The LC free bulk energy F is given by

$$F = \iiint_V F_b \, dV = \iiint_V \left(F_{\text{th}} + F_{\text{el}} + F_{\text{em}}\right) \, dV, \tag{3}$$

where F_b is the total energy density function and F_{th}, F_{el}, and F_{em} denote the thermotropic, elastic, and electromagnetic contributions, respectively. Strong homeotropic boundary conditions at the LC/polymer interfaces are applied.

The thermotropic energy F_{th} is expressed as $\mathbf{Q}$=$\mathbf{0}$

$$F_{\text{th}} = a\,\text{tr}\left(\mathbf{Q}^2\right) + \frac{2b}{3}\text{tr}\left(\mathbf{Q}^3\right) + \frac{c}{2}\left(\text{tr}\left(\mathbf{Q}^2\right)\right)^2, \tag{4}$$

where tr(.) denotes the trace of a matrix and the thermotropic coefficients are equal to $a = -0.3 \times 10^5$ J/m^3, $b = -1.5 \times 10^5$ J/m^3, and $c = 2.5 \times 10^5$ J/m^3 [30], thus yielding an equilibrium order parameter equal to $S_{\text{eq}} = 0.6$. The elastic energy stemming from the spatial distortion of the LC molecules, is given by

$$F_{\text{el}} = \sum_{i,j,k=1,2,3} \left[\frac{L_1}{2}\left(\frac{\partial Q_{ij}}{\partial x_k}\right)^2 + \frac{L_2}{2}\frac{\partial Q_{ij}}{\partial x_j}\frac{\partial Q_{ik}}{\partial x_k}\right] + \sum_{i,j,k,l=1,2,3} \left[\frac{L_6}{2} Q_{lk}\frac{\partial Q_{ij}}{\partial x_l}\frac{\partial Q_{ij}}{\partial x_k}\right]. \tag{5}$$

The elastic parameters L_i are related to the Frank elastic constants K_{ii} via the expressions $L_1 = (K_{33} - K_{11} + 3K_{22}) / \left(6S_{\text{exp}}^2\right)$, $L_2 = (K_{11} - K_{22}) / S_{\text{exp}}^2$, and $L_6 = (K_{33} - K_{11}) / \left(2S_{\text{exp}}^3\right)$. The Frank elastic constants for E7 are equal to $K_{11} = 10.3$ pN, $K_{22} = 7.4$ pN, and $K_{33} = 16.48$ pN [33] and we assume that the experimental nematic order parameter S_{exp} is equal to S_{eq}.

When an external electric field is applied, the electrostatic energy is given by

$$F_{\text{em}} = -\int \mathbf{D} \cdot d\mathbf{E}, \tag{6}$$

where $\mathbf{D}$ is the displacement and $\mathbf{E}$ the electric field. The displacement field is expressed via

$$\mathbf{D} = \varepsilon_0 \tilde{\varepsilon}_r \mathbf{E} + \mathbf{P}_s, \tag{7}$$

where ε_0 is the vacuum permittivity, $\tilde{\varepsilon}_r$ is the LC dielectric tensor and $\mathbf{P}_s$ is the spontaneous polarization vector. For nematic LC the dielectric tensor is related to the $\mathbf{Q}$-tensor via

$$\tilde{\varepsilon}_r = \Delta\varepsilon^* \mathbf{Q} + \bar{\varepsilon}\mathbf{I}, \tag{8}$$

where $\Delta\varepsilon^* = (\varepsilon_\parallel - \varepsilon_\perp)/S_{\text{exp}}$ is the scaled dielectric anisotropy and $\bar{\varepsilon} = (\varepsilon_\parallel + 2\varepsilon_\perp)/3$. The relative LC permittivities for E7 are $\varepsilon_\parallel = 18.6$ and $\varepsilon_\perp = 5.31$ [33].

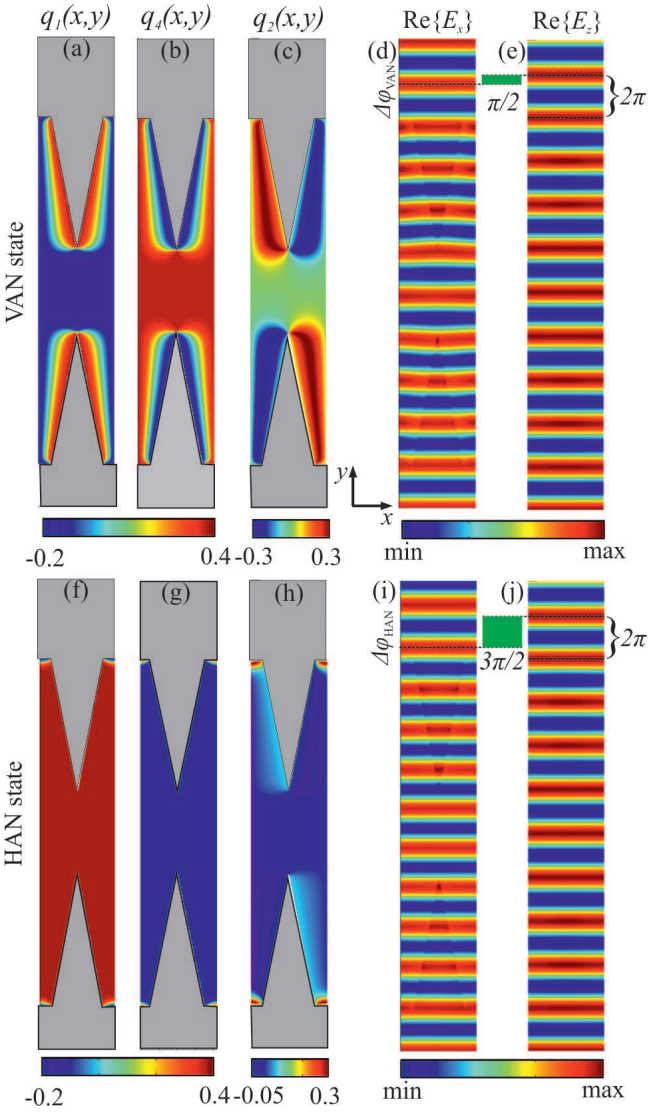

Figure 2. Profiles of the non-zero elements of the $Q-$tensor and the E_x and E_z components of the optical electric field for the (a-e) VAN and (f-j) HAN state at the wavelength of 1.55 µm. The phase difference accumulated between the two electric field components is 90° and 270° for the VAN and HAN states, respectively, as indicated by the green stripes and the wavefronts in (d,e) and (i,j). The geometrical parameters are: $p_0 = 0.9$ µm, $w_0 = 0.6$ µm, $a_0 = 3.074$ µm, and $h_0 = 8.128$ µm. The width profiles have been scaled by a factor of two for better viewing.

The spontaneous polarization derives from the flexoelectric effect, whose $i-$th component is given by

$$P_i = p_1 \sum_{j=1,2,3} \frac{\partial Q_{ij}}{\partial x_j} + p_2 \sum_{j,k=1,2,3} Q_{ij} \frac{\partial Q_{jk}}{\partial x_k}, \tag{9}$$

where $p_1 = (e_{11} + e_{33})/(2S_{\text{exp}})$ and $p_2 = (e_{11} - e_{33})/(2S_{\text{exp}}^2)$ are terms associated with the classical flexoelectric polarization coefficients e_{11} and e_{33}. For the case of E7, we consider the values $e_{11} = 12.5$ pC/m and $e_{33} = 2.5$ pC/m [34].

The free energy F is minimized by solving for the set of five Euler-Lagrange equations:

$$\sum_{j=1}^{3} \frac{\partial}{\partial x_j} \left(\frac{\partial F_b}{\partial q_{i,j}} \right) - \frac{\partial F_b}{\partial q_i} = \gamma_1^* \frac{\partial D}{\partial \dot{q}_i}, \tag{10}$$

for $i = 1...5$, where $q_{i,j} = \partial q_i / \partial x_j$, x_j being the unit vectors of the cartesian system. The r.h.s. of (10) describes the dynamic evolution of the $\mathbf{Q}$ tensor via the dissipation function $D = \text{tr}(\dot{\mathbf{Q}}^2)$, where $\dot{\mathbf{Q}} = \partial \mathbf{Q}/\partial t$. The term γ_1^* is associated with the rotational viscosity γ_1 via $\gamma_1^* = \gamma_1 / \left(4S_{\text{exp}}^2\right)$ [31], which for E7 is equal to 282.8 mPa·s [32].

3. Design of zenithal bistable grating circular polarizers

By simulating a wide range of combinations for the geometrical parameters, we have observed that the double grating supports two stable LC states. Figure 2 shows typical profiles of the non-zero elements of the Q-tensor for the VAN and HAN states. As in classical ZBD gratings, the LC director lies exclusively in the plane perpendicular to the groove axis. Therefore, zero values are implied for the elements q_3 and q_5, which are associated with the ε_{xz} and ε_{yz} elements of the dielectric permittivity tensor via (8) with $\varepsilon_{\parallel} = n_e^2$ and $\varepsilon_{\perp} = n_o^2$ being the LC extraordinary and ordinary permittivities at the investigated infrared spectrum.

The VAN state is characterized by low q_1 and therefore large tilt angle values across the LC cell, except for the lower-tilt regions around the triangular elements, owing to the LC homeotropic anchoring condition at the side walls of the grating. On the contrary, the HAN state shows an almost uniform zero-tilt profile, except from small regions at the troughs of the grating grooves, meaning that the LC orientation and thus the optical anisotropy axis is parallel to the x-axis in most of the bulk of the structure, with reference to Fig. 1.

The structure is excited with a plane wave at the target wavelength $\lambda_0 = 1.55$ µm that impinges perpendicularly to the substrate and it is linearly polarized at 45° with respect to the grating axis. The electric field can be decomposed into two components of equal amplitude polarized along the $x-$ and $z-$axis. Owing to the planar LC profiles, the E_z component senses a refractive index in the LC region equal to the ordinary index n_o irrespectively of the LC state. On the contrary, the E_x component senses an average index n_{av} as it propagates through the LC cell, which is between the ordinary and extraordinary LC index $n_o < n_{av} < n_e$. By examining the profiles shown in Fig. 2(a) and 2(f), it can be deduced that the average index in the VAN state is closer to n_o, while in the HAN state it is almost equal to n_e. At $\lambda_0 = 1.55$ µm

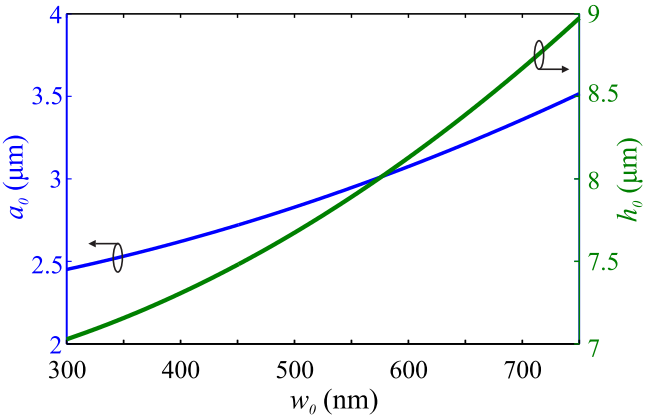

Figure 3. Sets of geometrical parameters optimized for operation as a switchable circular polarizer of the liquid-crystal zenithal bistable double grating. In all cases the pitch is set to $p_0 = 0.9$ µm.

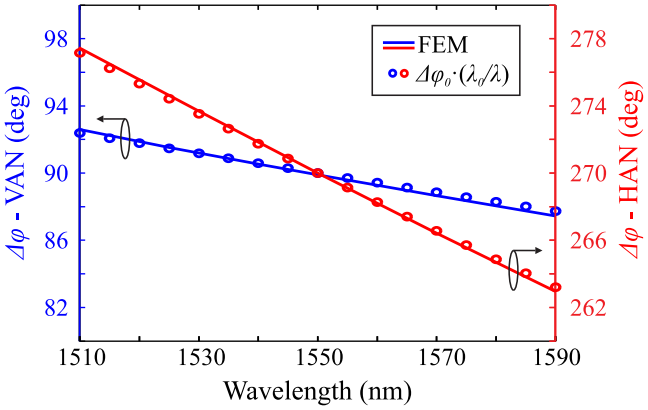

Figure 4. Phase difference $\Delta\varphi$ accumulated for the VAN and HAN states of the circular polarizer described in Fig. 2, in the spectral window between 1.5 and 1.6 µm.

the LC indices are $n_o = 1.5024$ and $n_e = 1.697$ [35]. Therefore, given that $n_{av} > n_o$, in both LC states a phase retardation $\Delta\varphi$ is accumulated for the E_x component with respect to E_z, with $\Delta\varphi$ being higher for the HAN state.

By properly selecting the geometrical parameters of the structure, we demonstrate that the value of $\Delta\varphi$ can be set at 90° and 270° for the VAN and HAN state, respectively, and thus the grating can operate as a switchable circular polarizer, where the switching between the two stable LC states selects the handedness of the output circular polarized plane wave. The profiles of the two optical electric field components for such an optimized geometry are shown in Fig. 2(d,e) and 2(i,j). All calculations have been performed by means of the finite-element method, implemented in the commercial software Comsol Multiphysics^{TM}. The corresponding parameters are $p_0 = 0.9$ µm, $w_0 = 0.6$ µm, $a_0 = 3.074$ µm, and $h_0 = 8.128$ µm. The sub-micron lattice pitch value ensures that all grating diffraction orders are suppressed. The polymer index is set to $n_p = 1.55$, which corresponds to SU-8 in the infrared telecom band [36], a typical negative photoresist employed in optical lithography microfabrication and nano-imprint lithography (NIL) [37]. Other suitable material options for the fabrication of the gratings include PMMA or PDMS, a conformable material suitable for NIL. The corresponding refractive indices of these two materials are approximately 1.49 and 1.40. Our analysis has shown that the choice of the grating material, although leading to noticeable changes in the n_p value, has a minor effect on the polarization conversion process which stems mainly from the LC optical anisotropy. The change of n_p is found to introduce a slight phase shift of the transmitted wave components and somewhat alter the Fresnel reflection. Even in the worst-case scenario of choosing the lowest-index material PDMS for the grating, which creates the maximum index contrast $n_e - n_p$, the Fresnel reflection losses are still below 1%.

Figure 3 shows the design parameters of the switchable polarizer for a constant pitch $p_0 = 0.9$ µm at the wavelength of 1.55 µm. First, for a given w_0 the triangle height a_0 that provides $\Delta\varphi = 90°$ for the VAN state is calculated. Subsequently, the LC cell thickness h_0 is adjusted such that the phase difference of 270° is accumulated for the HAN state. Since the lower-tilt zones for the VAN state are confined to the vicinity of the grating, the variation of h_0 does not influence the value of the accumulated phase for the VAN state, as it will be shown in Section III. Selecting small values of w_0 in general adds to the complexity of the fabrication process as high aspect ratios a_0/w_0 are required for the triangular features, in accordance with the results of Fig. 3. In the following of this work we study the geometry of Fig. 2, where $w_0 = 0.6$ µm. It is stressed that the same procedure can be applied in principle for any other target wavelength or polymer index, by adapting the grating geometry.

4. Performance of zenithal bistable grating circular polarizers

Considering that the proposed device is analogous to a quarter waveplate, its performance will depend on the wavelength of the incoming light as well as on the accuracy with which its geometrical features are reproduced in fabrication. The spectral dependence of the polarizing properties of the component are investigated in Fig. 4. The phase difference accumulated for both states is found to scale, to an excellent approximation, as λ_0/λ, which is typical of waveplates where the phase shift equals the ratio of the plate thickness and wavelength. In the case of

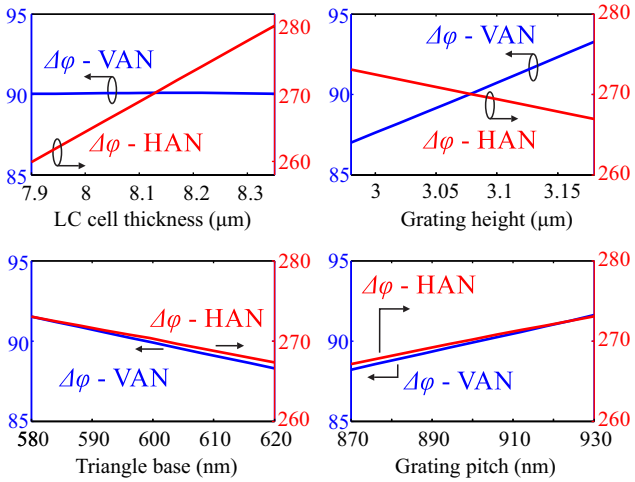

Figure 5. Performance of the circular polarizer of Fig. 2 at $\lambda_0 = 1.55$ μm for variations of the geometrical parameters away from the optimal values.

the VAN state, resonances have been observed at some lower wavelengths, outside the spectra window under study, owing to the coupling of x-polarized incident waves to y-polarized guided modes propagating along the grating axis (x-axis) [38]. This occurs when phase matching conditions are met, together with other particular conditions that allow for the excitation such modes, i.e. the existence of non-zero ε_{xy} elements and sufficiently high index contrast provided by the LC orientation in the VAN state.

Perhaps the critical aspect in developing the proposed ZBD-CP is a cost-effective fabrication of polymer gratings with specified high-aspect-ratio profiles. Using numerical calculations similar to those shown in Fig. 2, it can be directly shown that the key (in terms of HAN and VAN state formation) element of the assumed triangular grating is not the sharpness of its apex but the triangle sidewall angles. Grating profiles having aspect ratios of 5, as required by the parameters assumed in Fig. 2, (or even higher) are commercially available and can be routinely fabricated in silicon by combining various lithographic techniques with appropriate etching processes, the latter being decisive for achieving a desired sidewall angle [39]. Once the desired profile is reached with a silicon master, it can be transferred into an arbitrary number of replicas made of the desired polymer using nanoimprint lithography [40], thus rendering a large-scale fabrication of ZBD-CP devices cheap. This further implies that the four geometrical parameters defining the grating in Fig. 1, can be realistically fabricated if tolerances of few tens of nanometers are allowed.

The robustness of the ZBD-CP design in the parameter space that is realistic in terms of fabrication is demonstrated in Fig. 5. It shows the variation of $\Delta\phi$ values associated with HAN and VAN states with each of the four structural parameters, assuming that the other parameters have values as given in 2. As commented, the variation of the LC cell thickness influences only the HAN state by accordingly modifying the light propagation path, as in Fig. 5(a). Increasing the grating height h_0, as shown in Fig. 5(b), reduces the effective birefringence for the HAN state as low-tilt LC molecules become replaced by the grating polymer. In the VAN state, however, $\Delta\phi$ exhibits the opposite behavior, as in that case the incoming linearly polarized field experiences birefringence only in the vicinity of the grating surface (cf. Fig. 2) meaning that $\Delta\phi$ is proportional to the grating surface area and hence grows with h_0. Increasing the triangle basis in Fig. 5(c) has the effect of both reducing the small-tilt LC volume and the grating surface area and, consequently, results in the decrease of both the HAN and VAN $\Delta\phi$. Finally, as increasing the pitch in Fig. 5(d) is analogous to the decrease of the triangle base, it leads to the increase of both $\Delta\phi$. It is thus established that variations from the optimal values due to fabrication errors do not significantly affect the performance of the proposed polarizer, as its operation is not based on resonant phenomena but rather the phase retardation stems from an average interaction of the propagating E_x component with the LC in the entire cross-section of the cell.

The handedness of the output circularly polarized wave can be selected by alternating between the two LC states corresponding to local minima of the total LC energy. In the consolidated ZBD display technology, this can be achieved by applying a voltage across the LC cell, by means of a pair of uniform planar ITO electrodes, whose presence in the proposed structure does not influence the polarizing properties, since ITO is an isotropic material.

Depending on the amplitude, duration and polarity, the control pulse can mediate the transition between the VAN and HAN states. This procedure is governed by two effects, the dielectric and the flexoelectric coupling of the nematic director with the applied electric field. In the case of the flexoelectric switching being the dominant effect in switching, the response speed can be lowered [29, 30, 41] to sub-millisecond times with voltages below 10 V, when using optimized LC mixtures, which provide high $\Delta\varepsilon$ and low viscosities [42]. Conversely, when the dielectric effect rules, another possibility for switching is the use of dual-frequency LC materials, via the reversal of the sign of $\Delta\varepsilon$ by means of adjusting the frequency of the control voltage, which is a standard option for the control of LC-tunable devices including bistable LC cells and gratings [43].

In a preliminary study conducted for the case

of the ZBD polarizer studied in Fig. 2, we have observed switching between the two states by applying a rectangular voltage pulse across the LC cell. For a pulse duration $\tau = 5$ ms, HAN to VAN (VAN to HAN) switching was achieved for an applied voltage $V = 90$ V ($V = 70$ V) and transition times in the range of 10 ms (50 ms). For such indicative values, the energy required to switch the proposed polarizer assuming an active surface $S = 1$ cm^2, is estimated by $E_s \simeq CV_0^2 f\tau$, where $C \simeq \varepsilon_0\varepsilon_e S/h_0$ is the upper limit of the LC cell capacitance, and $f = 1$ KHz the control frequency, is in the order of tens of µJ. It is stressed that the device needs to consume energy only when the switching pulse is applied and not in idle operation in either of the two states.

5. Conclusions

We have presented the design methodology of a switchable circular polarizer based on a zenithal bistable liquid-crystal double grating, where the handedness of the output circular polarization can be selected by switching between the two bistable states of the grating. The component has been optimized for operation in the infrared telecom wavelengths, however the design methodology can be applied for any target wavelength and available materials. The spectral response of the polarizer, as well as the tolerance of its performance on the geometrical parameters of the grating have been investigated, revealing small dependences, owing to the non-resonant principle of operation.

Acknowledgments

This work was supported by the Italian Ministry of Foreign Affairs and International Cooperation, Directorate General for the Country Promotion (LC-NANOPLASM), and the Serbian Ministry of Education, Science and Technological Development under Project No. OI171005. The authors would also like to acknowledge the contribution of the COST Action IC1208.

References

[1] Zografopoulos D C, Asquini R, Kriezis E E, d'Alessandro A and Beccherelli R 2012 *Lab Chip* **12** 3598–3610
[2] Beeckman J, Neyts K and Vanbrabant P J M 2011 *Opt. Eng.* **50** 081202
[3] Zografopoulos D C, Kriezis E E, Bellini B and Beccherelli R 2007 *Opt. Express* **15** 1832–1844
[4] Donisi D, Bellini B, Beccherelli R, Asquini R, Gilardi G, Trotta M and d'Alessandro A 2010 *IEEE J. Quantum Electron.* **46** 762–768
[5] Zografopoulos D C and Beccherelli R 2013 *Opt. Express* **21** 8240–8250
[6] Alkeskjold T T, Lægsgaard J, Bjarklev A, Hermann D S, Broeng J, Li J and Wu S T 2004 *Opt. Express* **12** 5857–5871
[7] Zografopoulos D C and Kriezis E E 2009 *J. Lightwave Technol.* **27** 773–779
[8] Pitilakis A K, Zografopoulos D C and Kriezis E E 2011 *J. Lightwave Technol.* **29** 2560–2569
[9] Uche C, Elston S J and Parry-Jones L A 2005 *J. Phys. D: Appl. Phys.* **38** 2283–2291
[10] Tsakonas C, Davidson A J, Brown C V and Mottram N J 2007 *Appl. Phys. Lett.* **90** 111913
[11] Willman E, Fernández F A, James R and Day S E 2008 *J. Display Technol.* **4** 276–281
[12] Ladak S, Davidson A, Brown C V and Mottram N J 2009 *J. Phys. D: Appl. Phys.* **42** 085114
[13] Evans C R, Davidson A J, Brown C V and Mottram N J 2010 *J. Phys. D: Appl. Phys.* **43** 495105
[14] Jones C 2012 *Bistable Liquid Crystal Devices* vol 3 (Springer) chap 7.3.5 in *Handbook of Visual Display Technology*, pp 1507–1543
[15] Bryan-Brown G P, Brown C V and Jones J C 1995 *US Patent No. US6249332*
[16] Edwards E G, Brown C V, Kriezis E E, Elston S J, Kitson S C and Newton C J P 2004 *Mol. Cryst. Liq. Cryst.* **410** 401–408
[17] Spencer T J, Care C M, Amos R M and Jones J C 2010 *Phys. Rev. E* **82** 021702
[18] Jones J C 2006 *Proceedings of the SID* **51.2** 1626–1629
[19] Zografopoulos D C, Beccherelli R and Kriezis E E 2014 *Phys. Rev. E* **90** 042503
[20] Reisch A and Majumdar A 2014 *EPL* **107** 16002
[21] Zografopoulos D C and Kriezis E E 2014 *Opt. Lett.* **39** 5842–5845
[22] McManamon P F, Dorschner T A, Corkum D L, Friedman L J, Hobbs D S, Holz M, Liberman S, Nguyen H Q, Resler D P, Sharp R C, and Watson E A 1996 *Proc. IEEE* **84** 268–298
[23] Hsu W L, Davis J, Balakrishnan K, Ibn-Elhaj M, Kroto S, Brock N and Pau S 2015 *Opt. Express* **23** 4357–4368
[24] Bass M, Van Stryland E M, Williams D R, and Wolfe W L 1995 Handbook of Optics, 2nd ed., Vol. 2 (McGraw-Hill, New York)
[25] Lipton L 2001 *SMPTE Journal* **110** 586–593
[26] Cowan M, Greer J, Lipton L, and Chiu J 2007 *US Patent No. 2007/0258138 A1*
[27] Slussarenko S, Murauski A, Du T, Chigrinov V, Marrucci L and Santamato E 2011 *Opt. Express* **19** 4085–4090
[28] Stanciu C D, Hansteen F, Kimel A V, Kiriluk A, Tsukamoto A, Itoh A, and Rasing Th 1997 *Phys. Rev. Lett.* **99** 047601
[29] Brown C V, Parry-Jones L, Elston S J and Wilkins S J 2004 *Mol. Cryst. Liq. Cryst.* **410** 417–425
[30] Parry-Jones L A, Meyer R B and Elston S J 2009 *J. Appl. Phys.* **106** 014510
[31] Davidson A J, Brown C V, Mottram N J, Ladak S and Evans C R 2010 *Phys. Rev. E* **81** 051712
[32] Wang H, Wu T X, Gauza S, Wu J R and Wu S T *Liq. Cryst.* **33** 91–98
[33] Strömer J F, Raynes E P and Brown C V 2006 *Appl. Phys. Lett.* **88** 051915
[34] Buka Á and Éber N (eds) 2013 *Flexoelectricity in liquid crystals* (Imperial College Press)
[35] Li J, Wu S T, Brugioni S, Meucci R and Faetti S 2005 *J. Appl. Phys.* **97** 073501
[36] MicroChem Corp., (`http://www.microchem.com`).
[37] Guo L J 2007 *Adv. Mater.* **19** 495–513
[38] Yang F, Yen G, Rasigade G, Soares J A N T and Cunningham B T 2008 *Appl. Phys. Lett.* **92** 091115
[39] Hung J-Y, Lee S-L, Thibeault B-J and Coldren L-A 2011 *IEEE J. Sel. Top. Quantum Electron.* **17** 869–877

[40] Chou S-Y, Krauss P-R and Renstrom P-J 1996 *J. Vac. Sci. Technol. B* **14** 4129–4133
[41] Jones J C, Beldon S, Brett P, Francis M and Goulding M 2003 *Proceedings of the SID* **26.3** 954–957
[42] Francis M, Goulding M J, Jones J C and Beldon S 2006 *US Patent No. 2006/0115603 A1*
[43] Palto S P and Barnik M I 2006 *J. Exp. Theor. Phys.* **102** 998–1007